Dyadic Green's functions and guided surface waves for a surface conductivity model of graphene

George W. Hanson[a)]
Department of Electrical Engineering, University of Wisconsin-Milwaukee, 3200 N. Cramer St., Milwaukee, Wisconsin 53211, USA

(Received 3 August 2007; accepted 9 January 2008; published online 18 March 2008)

An exact solution is obtained for the electromagnetic field due to an electric current in the presence of a surface conductivity model of graphene. The graphene is represented by an infinitesimally thin, local, and isotropic two-sided conductivity surface. The field is obtained in terms of dyadic Green's functions represented as Sommerfeld integrals. The solution of plane wave reflection and transmission is presented, and surface wave propagation along graphene is studied via the poles of the Sommerfeld integrals. For isolated graphene characterized by complex surface conductivity $\sigma = \sigma' + j\sigma''$, a proper transverse-electric surface wave exists if and only if $\sigma'' > 0$ (associated with interband conductivity), and a proper transverse-magnetic surface wave exists for $\sigma'' < 0$ (associated with intraband conductivity). By tuning the chemical potential at infrared frequencies, the sign of σ'' can be varied, allowing for some control over surface wave properties. © *2008 American Institute of Physics*. [DOI: 10.1063/1.2891452]

I. INTRODUCTION

Fundamental properties and potential applications of carbon-based structures are of interest in emerging nanoelectronic applications. Particularly promising is graphene, which is a planar atomic layer of carbon atoms bonded in a hexagonal structure. Graphene is the two-dimensional version of graphite, and a single-wall carbon nanotube can be thought of as graphene rolled into a tube.[1]

Only recently has it become possible to fabricate ultrathin graphite, consisting of only a few graphene layers,[2,3] and actual graphene.[4–8] In graphene, the energy-momentum relationship for electrons is linear over a wide range of energies, rather then quadratic, so that electrons in graphene behave as massless relativistic particles (Dirac fermions) with an energy-independent velocity. Graphene's band structure, together with its extreme thinness, leads to a pronounced electric field effect,[5,9] which is the variation of a material's carrier concentration with electrostatic gating. This is the governing principle behind traditional semiconductor device operation, and therefore this effect in graphene is particularly promising for the development of ultrathin carbon nanoelectronic devices. Although the electric field effect also occurs in atomically thin metal films, these tend to be thermodynamically unstable and do not form continuous layers with good transport properties. In contrast, graphene is stable, and, like its cylindrical carbon nanotube versions, can exhibit ballistic transport over at least submicron distances.[5] Furthermore, it has been shown that graphene's conductance has a minimum, nonzero value associated with the conductance quantum, even when charge carrier concentrations vanish.[6]

In this work, the interaction of an electromagnetic current source and graphene is considered. The electromagnetic fields are governed by Maxwell's equations, and the graphene is represented by a conductivity surface[10] that must arise from a microscopic quantum-dynamical model or from measurement. The method assumes laterally infinite graphene residing at the interface between two dielectrics, in which case classical Maxwell's equations are solved exactly for an arbitrary electrical current. Related phenomena are discussed, such as plane wave reflection and transmission through graphene,[11] and surface wave excitation and guidance, which is relevant to high-frequency electronic applications. It is found that the relative importance of the interband and intraband contributions to the conductivity dictate surface wave behavior,[12] and that surface wave propagation can be controlled by varying the chemical potential.

Although at this time only graphene samples with lateral dimensions on the order of tens of microns have been fabricated, the infinite sheet model provides a first step in analyzing electromagnetic properties of graphene. It is also relevant to sufficiently large finite-sized sheets, assuming that electronic edge effects and electromagnetic edge diffraction can be ignored. In the following all units are in the SI system, and the time variation (suppressed) is $e^{j\omega t}$, where j is the imaginary unit.

II. FORMULATION OF THE MODEL

A. Electronic model of graphene

Figure 1 depicts laterally infinite graphene lying in the $x-z$ plane at the interface between two different mediums characterized by μ_1, ε_1 for $y \geq 0$ and μ_2, ε_2 for $y < 0$, where all material parameters may be complex-valued.

The graphene is modeled as an infinitesimally thin, local two-sided surface characterized by a surface conductivity $\sigma(\omega, \mu_c, \Gamma, T)$, where ω is radian frequency, μ_c is chemical potential, Γ is a phenomenological scattering rate that is assumed to be independent of energy ε, and T is temperature.

[a)]Electronic mail: george@uwm.edu.

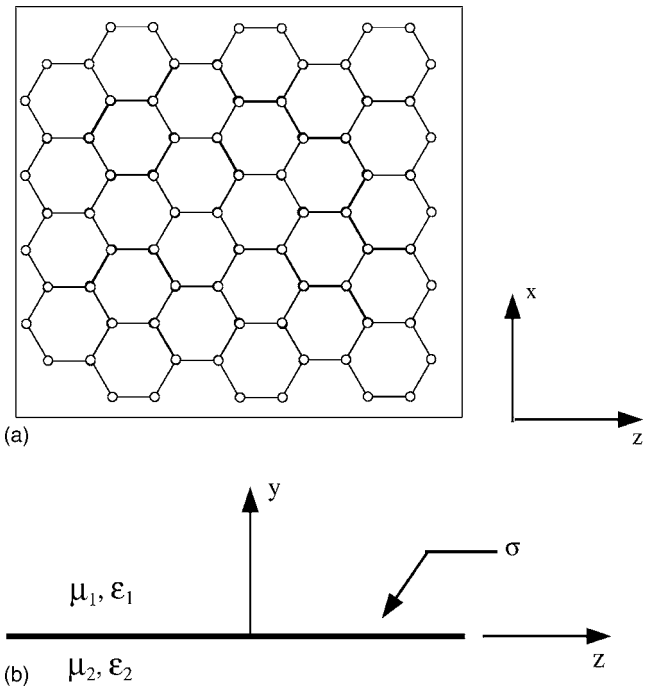

FIG. 1. (a) Depiction of graphene (top view), where the small circles denote carbon atoms, and (b) graphene characterized by conductance σ at the interface between two dielectrics (side view).

The conductivity of graphene has been considered in several recent works,[11–18] and here we use the expression resulting from the Kubo formula,[19]

$$\sigma(\omega,\mu_c,\Gamma,T) = \frac{je^2(\omega-j2\Gamma)}{\pi\hbar^2}\left[\frac{1}{(\omega-j2\Gamma)^2}\int_0^\infty \varepsilon\left(\frac{\partial f_d(\varepsilon)}{\partial\varepsilon}-\frac{\partial f_d(-\varepsilon)}{\partial\varepsilon}\right)d\varepsilon - \int_0^\infty \frac{f_d(-\varepsilon)-f_d(\varepsilon)}{(\omega-j2\Gamma)^2-4(\varepsilon/\hbar)^2}d\varepsilon\right], \quad (1)$$

where $-e$ is the charge of an electron, $\hbar=h/2\pi$ is the reduced Planck's constant, $f_d(\varepsilon)=(e^{(\varepsilon-\mu_c)/k_BT}+1)^{-1}$ is the Fermi-Dirac distribution, and k_B is Boltzmann's constant. We assume that no external magnetic field is present, and so the local conductivity is isotropic (i.e., there is no Hall conductivity). The first term in Eq. (1) is due to intraband contributions, and the second term to interband contributions.

For an isolated graphene sheet the chemical potential μ_c is determined by the carrier density n_s,

$$n_s = \frac{2}{\pi\hbar^2 v_F^2}\int_0^\infty \varepsilon[f_d(\varepsilon)-f_d(\varepsilon+2\mu_c)]d\varepsilon, \quad (2)$$

where $v_F\simeq 9.5\times 10^5$ m/s is the Fermi velocity. The carrier density can be controlled by application of a gate voltage and/or chemical doping. For the undoped, ungated case at $T=0$ K, $n_s=\mu_c=0$.

The intraband term in Eq. (1) can be evaluated as

$$\sigma_{intra}(\omega,\mu_c,\Gamma,T) = -j\frac{e^2k_BT}{\pi\hbar^2(\omega-j2\Gamma)}\left(\frac{\mu_c}{k_BT}+2\ln(e^{-\mu_c/k_BT}+1)\right). \quad (3)$$

For the case $\mu_c=0$, Eq. (3) was first derived in Ref. 20 for graphite (with the addition of a factor to account for the interlayer separation between graphene planes) and corresponds to the intraband conductivity of a single-wall carbon nanotube in the limit of infinite radius.[10] With $\sigma=\sigma'+j\sigma''$, it can be seen that $\sigma'_{intra}\geq 0$ and $\sigma''_{intra}<0$. As will be discussed later, the imaginary part of conductivity plays an important role in the propagation of surface waves guided by the graphene sheet.[12]

The interband conductivity can be approximated for $k_BT\ll|\mu_c|,\hbar\omega$ as[21]

$$\sigma_{inter}(\omega,\mu_c,\Gamma,0)\simeq\frac{-je^2}{4\pi\hbar}\ln\left(\frac{2|\mu_c|-(\omega-j2\Gamma)\hbar}{2|\mu_c|+(\omega-j2\Gamma)\hbar}\right), \quad (4)$$

such that for $\Gamma=0$ and $2|\mu_c|>\hbar\omega$, $\sigma_{inter}=j\sigma''_{inter}$ with $\sigma''_{inter}>0$. For $\Gamma=0$ and $2|\mu_c|<\hbar\omega$, σ_{inter} is complex-valued, with[22]

$$\sigma'_{inter}=\frac{\pi e^2}{2h}=\sigma_{\min}=6.085\times 10^{-5}\ (\mathrm{S}), \quad (5)$$

and $\sigma''_{inter}>0$ for $\mu_c\neq 0$.

B. Dyadic Green's function for a surface model of graphene

For any planarly layered, piecewise-constant medium, the electric and magnetic fields in region n due to an electric current can be obtained as[23,24]

$$\mathbf{E}^{(n)}(\mathbf{r})=(k_n^2+\nabla\nabla)\pi^{(n)}(\mathbf{r}), \quad (6)$$

$$\mathbf{H}^{(n)}(\mathbf{r})=j\omega\varepsilon_n\nabla\times\pi^{(n)}(\mathbf{r}), \quad (7)$$

where $k_n=\omega\sqrt{\mu_n\varepsilon_n}$ and $\pi^{(n)}(\mathbf{r})$ are the wavenumber and electric Hertzian potential in region n, respectively. Assuming that the current source is in region 1, then

$$\pi^{(1)}(\mathbf{r})=\pi_1^p(\mathbf{r})+\pi_1^s(\mathbf{r}) = \int_\Omega\left[\underline{\mathbf{g}}_1^p(\mathbf{r},\mathbf{r}')+\underline{\mathbf{g}}_1^s(\mathbf{r},\mathbf{r}')\right]\frac{\mathbf{J}^{(1)}(\mathbf{r}')}{j\omega\varepsilon_1}d\Omega', \quad (8)$$

$$\pi^{(2)}(\mathbf{r})=\pi_2^s(\mathbf{r})=\int_\Omega\underline{\mathbf{g}}_2^s(\mathbf{r},\mathbf{r}')\frac{\mathbf{J}^{(1)}(\mathbf{r}')}{j\omega\varepsilon_1}d\Omega', \quad (9)$$

where the underscore indicates a dyadic quantity, and where Ω is the support of the current. With y parallel to the interface normal, the principle Green's dyadic can be written as[23]

$$\underline{\mathbf{g}}_1^p(\mathbf{r},\mathbf{r}')=\underline{\mathbf{I}}\frac{e^{-jk_1R}}{4\pi R}=\underline{\mathbf{I}}\frac{1}{2\pi}\int_{-\infty}^{\infty}e^{-p_1|y-y'|}\frac{H_0^{(2)}(k_\rho\rho)}{4p_1}k_\rho\,dk_\rho, \quad (10)$$

where

$$p_n^2 = k_\rho^2 - k_n^2, \quad \rho = \sqrt{(x-x')^2 + (z-z')^2},$$

$$R = |\mathbf{r} - \mathbf{r}'| = \sqrt{(y-y')^2 + \rho^2}, \tag{11}$$

and where k_ρ is a radial wavenumber and $\underline{\mathbf{I}}$ is the unit dyadic.

The scattered Green's dyadics can be obtained by enforcing the usual electromagnetic boundary conditions

$$\mathbf{y} \times (\mathbf{H}_1 - \mathbf{H}_2) = \mathbf{J}_e^s,$$

$$\mathbf{y} \times (\mathbf{E}_1 - \mathbf{E}_2) = -\mathbf{J}_m^s, \tag{12}$$

where $\mathbf{J}_e^s$ (A/m) and $\mathbf{J}_m^s$ (V/m) are electric and magnetic surface currents on the boundary. For a local model of graphene in the absence of a magnetic field and associated Hall effect conductivity, σ is a scalar. Therefore,[10]

$$J_{e,x}^s(x, y=0, z) = \sigma E_x(x, y=0, z), \tag{13}$$

$$J_{e,z}^s(x, y=0, z) = \sigma E_z(x, y=0, z), \tag{14}$$

$$\mathbf{J}_m^s(x, y=0, z) = \mathbf{0}, \tag{15}$$

and Eq. (12) becomes

$$E_{1,\alpha}(y=0^+) = E_{2,\alpha}(y=0^-), \quad \alpha = x, z, \tag{16}$$

$$H_{2,x}(y=0^-) - H_{1,x}(y=0^+) = \sigma E_z(y=0), \tag{17}$$

$$H_{2,z}(y=0^-) - H_{1,z}(y=0^+) = -\sigma E_x(y=0). \tag{18}$$

Using Eq. (6), the boundary conditions on the Hertzian potential at $(x, y=0, z)$ are

$$\pi_{1,\alpha} = N^2 M^2 \pi_{2,\alpha}, \tag{19}$$

$$\varepsilon_1 \pi_{1,y} - \varepsilon_2 \pi_{2,y} = \frac{\sigma}{j\omega} \nabla \cdot \pi_1 \tag{20}$$

$$\varepsilon_2 \frac{\partial \pi_{2,\alpha}}{\partial y} - \varepsilon_1 \frac{\partial \pi_{1,\alpha}}{\partial y} = \frac{\sigma}{j\omega} k_1^2 \pi_{1,\alpha} \tag{21}$$

$$\left(\frac{\partial \pi_{1,y}}{\partial y} - \frac{\partial \pi_{2,y}}{\partial y} \right) = (1 - N^2 M^2) \left(\frac{\partial \pi_{2,x}}{\partial x} + \frac{\partial \pi_{2,z}}{\partial z} \right), \tag{22}$$

$\alpha = x, z$, where $N^2 = \varepsilon_2/\varepsilon_1$ and $M^2 = \mu_2/\mu_1$. In the absence of magnetic contrast (e.g., if $M=1$) and surface conductivity, boundary conditions Eqs. (19)–(22) are identical to the Hertzian potential boundary conditions presented.[25]

Enforcing Eqs. (19)–(22) and following the method described in Ref. 25, the scattered Green's dyadic is found to be

$$\underline{\mathbf{g}}_1^s(\mathbf{r}, \mathbf{r}') = \hat{\mathbf{y}}\hat{\mathbf{y}} g_n^s(\mathbf{r}, \mathbf{r}') + \left(\hat{\mathbf{y}}\hat{\mathbf{x}} \frac{\partial}{\partial x} + \hat{\mathbf{y}}\hat{\mathbf{z}} \frac{\partial}{\partial z} \right) g_c^s(\mathbf{r}, \mathbf{r}') + (\hat{\mathbf{x}}\hat{\mathbf{x}} + \hat{\mathbf{z}}\hat{\mathbf{z}}) g_t^s(\mathbf{r}, \mathbf{r}'), \tag{23}$$

where the Sommerfeld integrals are

$$g_\beta^s(\mathbf{r}, \mathbf{r}') = \frac{1}{2\pi} \int_{-\infty}^{\infty} R_\beta \frac{H_0^{(2)}(k_\rho \rho) e^{-p_1(y+y')}}{4p_1} k_\rho \, dk_\rho, \tag{24}$$

$\beta = t, n, c$, with

$$R_t = \frac{M^2 p_1 - p_2 - j\sigma\omega\mu_2}{M^2 p_1 + p_2 + j\sigma\omega\mu_2} = \frac{N^H(k_\rho, \omega)}{Z^H(k_\rho, \omega)}, \tag{25}$$

$$R_n = \frac{N^2 p_1 - p_2 + \frac{\sigma p_1 p_2}{j\omega\varepsilon_1}}{N^2 p_1 + p_2 + \frac{\sigma p_1 p_2}{j\omega\varepsilon_1}} = \frac{N^E(k_\rho, \omega)}{Z^E(k_\rho, \omega)}, \tag{26}$$

$$R_c = \frac{2p_1 \left[(N^2 M^2 - 1) + \frac{\sigma p_2 M^2}{j\omega\varepsilon_1} \right]}{Z^H Z^E}, \tag{27}$$

which reduce to the previously known results as $\sigma \to 0$.

The Green's dyadic for region 2, $\underline{\mathbf{g}}_2^s(\mathbf{r}, \mathbf{r}')$, has the same form as for region 1, although in Eq. (24) the replacement

$$R_\beta e^{-p_1(y+y')} \to T_\beta e^{p_2 y} e^{-p_1 y'} \tag{28}$$

must be made, where

$$T_t = \frac{(1 + R_t)}{N^2 M^2} = \frac{2p_1}{N^2 Z^H}, \tag{29}$$

$$T_n = \frac{p_1(1 - R_n)}{p_2} = \frac{2p_1}{Z^E}, \tag{30}$$

$$T_c = \frac{2p_1 \left[(N^2 M^2 - 1) + \frac{\sigma p_1}{j\omega\varepsilon_1} \right]}{N^2 Z^H Z^E}. \tag{31}$$

As in the case of a simple dielectric interface, the denominators $Z^{H,E}(k_\rho, \omega) = 0$ implicate pole singularities in the spectral plane associated with surface wave phenomena. Furthermore, both wave parameters $p_n = \sqrt{k_\rho^2 - k_n^2}$, $n=1, 2$, lead to branch points at $k_\rho = \pm k_n$, and thus the k_ρ-plane is a four-sheeted Riemann surface. The standard hyperbolic branch cuts[24] that separate the one proper sheet [where $\mathrm{Re}(p_n) > 0$, such that the radiation condition as $|y| \to \infty$ is satisfied] and the three improper sheets [where $\mathrm{Re}(p_n) < 0$] are the same as in the absence of surface conductivity σ.

In addition to representing the exact field from a given current, several interesting electromagnetic aspects of graphene can be obtained from the above relations.

C. Plane wave reflection and transmission coefficients

Normal incidence plane wave reflection and transmission coefficients can be obtained from the previous formulation by setting $k_\rho = 0$ in Eqs. (25) and (29). To see this, consider the current

$$\mathbf{J}^{(1)}(\mathbf{r}) = \hat{\alpha} \frac{j4\pi r_0}{\omega\mu_1} \delta(\mathbf{r} - \mathbf{r}_0), \tag{32}$$

where $\hat{\alpha} = \hat{\mathbf{x}}$ or $\hat{\mathbf{y}}$, $\mathbf{r}_0 = \hat{\mathbf{y}} y_0$, and where $y_0 \gg 0$. This current leads to a unit-amplitude, $\hat{\alpha}$-polarized, transverse electromagnetic plane wave, normally incident on the interface. The far scattered field in region 1, which is the reflected field, can be obtained by evaluating the spectral integral Eq. (24) using the method of steepest descents, which leads to the reflected field $\mathbf{E}^r = \hat{\alpha}\Gamma e^{-jk_1 y}$, where the reflection coefficient is $\Gamma = R_t(k_\rho = 0)$. In a similar manner, the far scattered field in region 2, the transmitted field, is obtained as $\mathbf{E}^t = \hat{\alpha} T e^{jk_2 y}$, where the transmission coefficient is $T = (1 + \Gamma)$. Therefore,

$$\Gamma = \frac{\eta_2 - \eta_1 - \sigma\eta_1\eta_2}{\eta_2 + \eta_1 + \sigma\eta_1\eta_2}, \tag{33}$$

$$T = (1 + R_t) = \frac{2\eta_2}{(\eta_2 + \eta_1 + \sigma\eta_1\eta_2)}, \tag{34}$$

where $\eta_n = \sqrt{\mu_n/\varepsilon_n}$ is the wave impedance in region n. The plane wave reflection and transmission coefficients obviously reduce to the correct results for $\sigma=0$, and in the limit $\sigma\to\infty$, $\Gamma\to -1$ and $T\to 0$ as expected.

In the special case $\varepsilon_1=\varepsilon_2=\varepsilon_0$ and $\mu_1=\mu_2=\mu_0$,

$$\Gamma = -\frac{\frac{\sigma\eta_0}{2}}{1+\frac{\sigma\eta_0}{2}}, \quad T = \frac{1}{\left(1+\frac{\sigma\eta_0}{2}\right)}, \tag{35}$$

where $\eta_0 = \sqrt{\mu_0/\varepsilon_0} \simeq 377\ \Omega$. The reflection coefficient agrees with the result presented in Ref. 11 for normal incidence.

D. Surface waves guided by graphene

Pole singularities in the Sommerfeld integrals represent discrete surface waves guided by the medium.[23,24] From Eqs. (25)–(27) and (29)–(31), the dispersion equation for surface waves that are transverse-electric (TE) to the propagation direction ρ (also known as H-waves) is

$$Z^H(k_\rho,\omega) = M^2 p_1 + p_2 + j\sigma\omega\mu_2 = 0, \tag{36}$$

whereas for transverse-magnetic (TM) waves (E-waves),

$$Z^E(k_\rho,\omega) = N^2 p_1 + p_2 + \frac{\sigma p_1 p_2}{j\omega\varepsilon_1} = 0. \tag{37}$$

In the limit that $\varepsilon_1=\varepsilon_2=\varepsilon_0$, $Z^{H,E}$ agree with TE and TM dispersion equations in Ref. 12.

The surface wave field can be obtained from the residue contribution of the Sommerfeld integrals. For example, the electric field in region 1 associated with the surface wave excited by a Hertzian dipole current $\mathbf{J}(\mathbf{r}) = \hat{\mathbf{y}} A_0 \delta(x)\delta(y)\delta(z)$ is

$$\mathbf{E}^{(1)}(\rho_0) = \frac{A_0 k_\rho^2 R_n'}{4\omega\varepsilon_1} e^{-p_1 y}\left[\left(\hat{\mathbf{x}}\frac{x}{\rho_0} + \hat{\mathbf{z}}\frac{z}{\rho_0}\right)H_0^{(2)\prime}(k_\rho\rho_0) - \hat{\mathbf{y}}\frac{(k_1^2+p_1^2)H_0^{(2)}(k_\rho\rho_0)}{k_\rho\sqrt{k_1^2-k_\rho^2}}\right],$$

where $R_n' = N^E/(\partial Z^E/\partial k_\rho)$, $H_0^{(2)\prime}(\alpha) = \partial H_0^{(2)}(\alpha)/\partial\alpha$, and $\rho_0 = \sqrt{x^2+z^2}$. The term $e^{-p_1 y}$ leads to exponential decay away from the graphene surface on the proper sheet [$\mathrm{Re}(p_n) > 0, \quad n=1,2$]. The surface wave mode may or may not lie on the proper Riemann sheet, depending on the value of surface conductivity, as described below. In general, only modes on the proper sheet directly result in physical wave phenomena, although leaky modes on the improper sheet can be used to approximate parts of the spectrum in restricted spatial regions, and to explain certain radiation phenomena.[26]

1. Transverse-electric surface waves

Noting that $p_2^2 - p_1^2 = k_0^2(\mu_1^r\varepsilon_1^r - \mu_2^r\varepsilon_2^r)$, where μ_n^r and ε_n^r are the relative material parameters (i.e., $\mu_n = \mu_n^r\mu_0$ and $\varepsilon_n = \varepsilon_n^r\varepsilon_0$) and $k_0^2 = \omega^2\mu_0\varepsilon_0$ is the free-space wavenumber, then, if $M=1$ ($\mu_1^r=\mu_2^r=\mu_r$), the TE dispersion Eq. (36) can be solved for the radial surface wave propagation constant, yielding

$$k_\rho = k_0\sqrt{\mu_r\varepsilon_1^r - \left(\frac{(\varepsilon_1^r-\varepsilon_2^r)\mu_r + \sigma^2\eta_0^2\mu_r^2}{2\sigma\eta_0\mu_r}\right)^2}. \tag{38}$$

If, furthermore, $N=1$ ($\varepsilon_1^r=\varepsilon_2^r=\varepsilon_r$), then Eq. (38) reduces to

$$k_\rho = k_0\sqrt{\mu_r\varepsilon_r - \left(\frac{\sigma\eta_0\mu_r}{2}\right)^2}. \tag{39}$$

For the case $M\neq 1$, then Eq. (36) leads to

$$k_\rho = k_0\sqrt{\mu_1^r\varepsilon_1^r - \frac{1}{(M^4-1)^2}\left(M^2\sigma\eta_0\mu_2^r \mp \sqrt{(\sigma\eta_0\mu_2^r)^2 - (M^4-1)(\varepsilon_1^r\mu_1^r - \varepsilon_2^r\mu_2^r)}\right)^2}. \tag{40}$$

Considering the special case of graphene in free-space, setting $\varepsilon_1^r=\varepsilon_2^r=\mu_1^r=\mu_2^r=1$,

$$k_\rho = k_0\sqrt{1-\left(\frac{\sigma\eta_0}{2}\right)^2}. \tag{41}$$

If σ is real-valued ($\sigma=\sigma'$) and $(\sigma'\eta_0/2)^2<1$, then a fast propagating mode exists, and if $(\sigma'\eta_0/2)^2>1$, the wave is either purely attenuating or growing in the radial direction. However, in both cases $p_n = p_0 = \sqrt{(k_\rho)^2 - k_0^2} = -j\sigma'\omega\mu_0/2$ from Eq. (36), and so $\mathrm{Re}(p_0)>0$ is violated. Therefore, for isolated graphene with σ real-valued (i.e., when $\sigma=\sigma_{\min}$, at low temperatures and small μ_c), all TE modes are on the improper Riemann sheet. The fast leaky mode may play a role in radiation from the structure.

If the conductivity is pure imaginary, $\sigma=j\sigma''$, then $k_\rho > k_0$ and a slow wave exists. In this case $p_0 = \sigma''\omega\mu_0/2$ and, if $\sigma''>0$, then $\mathrm{Re}(p_0)>0$ and the wave is a slow surface wave on the proper sheet. This will occur when the interband conductivity dominates over the intraband contribution, as described in Ref. 12. However, if $\sigma''<0$, which occurs when the intraband contribution dominates, the mode is exponentially growing in the vertical direction and is a leaky wave on the improper sheet.

More generally, for complex conductivity,

$$p_0 = \frac{-j\sigma\omega\mu_0}{2} = (\sigma'' - j\sigma')\frac{\omega\mu_0}{2}, \tag{42}$$

and, therefore, if $\sigma'' < 0$, the mode is on the improper sheet, whereas if $\sigma'' > 0$, a surface wave on the proper sheet is obtained.

2. Transverse-magnetic surface waves

TM waves are governed by the dispersion (37). For general material parameters this relation is more complicated than for the TE case, and so here we concentrate on an isolated graphene surface ($\varepsilon_1^r = \varepsilon_2^r = \mu_1^r = \mu_2^r = 1$). Then, $p_0 = -j2\omega\varepsilon_0/\sigma$ and

$$k_\rho = k_0\sqrt{1 - \left(\frac{2}{\sigma\eta_0}\right)^2}. \tag{43}$$

If σ is real-valued, then $\mathrm{Re}(p_0) > 0$ is violated and TM modes are on the improper Riemann sheet.

If conductivity is pure imaginary, then $k_\rho > k_0$ and a slow wave exists. Since $p_0 = -2\omega\varepsilon_0/\sigma''$, if $\sigma'' > 0$, then the wave is on the improper sheet, and, if $\sigma'' < 0$, the mode is a slow surface wave on the proper sheet. For complex conductivity,

$$p_0 = \frac{-j2\omega\varepsilon_0}{\sigma} = \frac{-2\omega\varepsilon_0}{|\sigma|^2}(\sigma'' + j\sigma'), \tag{44}$$

and, therefore, if $\sigma'' < 0$ (intraband conductivity dominates), the mode is a surface wave on the proper sheet, whereas, if $\sigma'' > 0$ (interband conductivity dominates), the mode is on the improper sheet.

In summary, for isolated grapheme, a proper TE surface wave exists if $\sigma'' > 0$, resulting in the radial wavenumber (41), and a proper TM surface wave with wavenumber (43) is obtained for $\sigma'' < 0$. The same conclusions hold for graphene in a homogeneous dielectric. For graphene with $\sigma'' = 0$, no surface wave propagation is possible. Note that this only refers to wave-propagation effects; dc or low-frequency transport between electrodes can occur, leading to electronic device possibilities. In fact, in devices not based on wave phenomena, the absence of surface waves is usually beneficial, as spurious radiation and coupling effects, and the associated degradation of device performance, are often associated with surface wave excitation.

The degree of confinement of the surface wave to the graphene layer can be gauged by defining an attenuation length ζ, at which point the wave decays to $1/e$ of its value on the surface. For graphene embedded in a homogeneous medium characterized by ε and μ, $\zeta^{-1} = \mathrm{Re}(p)$, leading to $\zeta^{TE} = 2/\sigma''\omega\mu$ $(\sigma'' > 0)$ and $\zeta^{TM} = -|\sigma|^2/2\omega\varepsilon\sigma''$ $(\sigma'' < 0)$. When normalized to wavelength,

$$\frac{\zeta^{TE}}{\lambda} = \frac{1}{\pi\eta\sigma''}, \quad \sigma'' > 0, \tag{45}$$

$$\frac{\zeta^{TM}}{\lambda} = -\frac{\eta|\sigma|^2}{4\pi\sigma''}, \quad \sigma'' < 0. \tag{46}$$

Obviously, strong confinement arises from large imaginary conductivity, as would be expected.

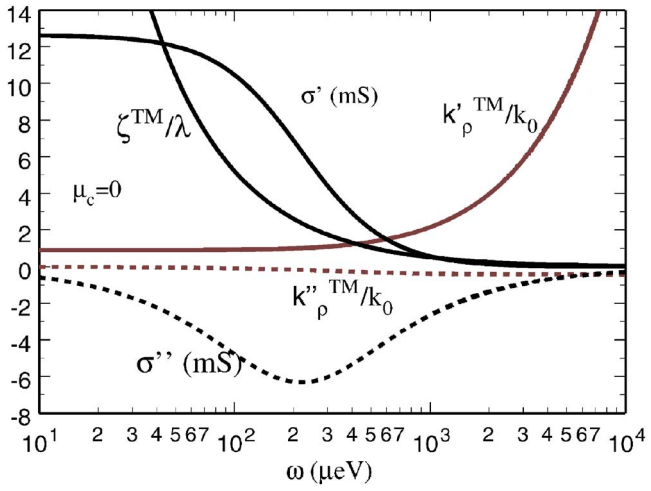

FIG. 2. (Color online) Complex conductivity, TM surface-wave wavenumber, and attenuation length for $\mu_c = 0$ at 300 K in the microwave through far-infrared frequency range ($\omega = 15.2$ GHz to 15.2 THz).

III. RESULTS

In this section, some results are shown for surface wave characteristics of graphene in the microwave and infrared regimes. In all cases $\Gamma = 0.11$ meV, $T = 300$ K, and an isolated graphene surface (i.e., when the surrounding medium is vacuum) is considered. The value of the scattering rate is chosen to be approximately the same as for electron-acoustic phonon interactions in single-wall carbon nanotubes.[27]

We first consider the case of zero chemical potential at microwave and far-infrared wave frequencies. Figure 2 shows the complex conductivity, TM surface-wave wavenumber (43) and attenuation length (46). In this case the intraband conductivity is dominant over the interband contribution, and so $\sigma'' < 0$, such that only a TM surface wave can exist. The dispersion of the complex conductivity follows simply from the Drude form (3). At low frequencies the TM surface wave is poorly confined to the graphene surface ($\zeta^{TM}/\lambda \gg 1$), and therefore it is lightly damped and relatively fast (i.e., $k_\rho^{TM}/k_0 \simeq 1$). As frequency increases into the far-infrared, the surface wave becomes more tightly confined to the graphene layer, but becomes slow as energy is concentrated on the graphene surface.

The conductivity can be varied by adjusting the chemical potential, which is governed by the carrier density via Eq. (2). The carrier density can be changed by either chemical doping or by the application of a bias voltage. Figure 3 shows the intraband and interband conductivity as a function of chemical potential for $\omega = 6.58$ μeV ($\omega = 10$ GHz). As expected, the conductivity increases with increasing chemical potential, associated with a higher carrier density n_s. Because intraband conductivity is dominant, σ'' remains negative as chemical potential is varied, and therefore only a TM surface wave may propagate. The inset shows the real part of the intraband conductivity (the dominant term) on a linear scale, showing the linear dependence of σ on μ_c.

Since the TM surface wave is not well confined to the graphene surface at lower microwave frequencies, it undergoes little dispersion with respect to chemical potential. This is illustrated in Fig. 4, where the TM wavenumber and at-

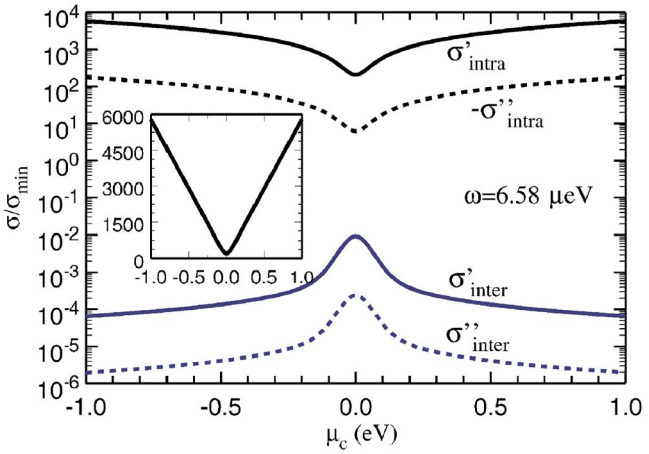

FIG. 3. (Color online) Intraband and interband conductivity as a function of chemical potential at $T=300$ K, $\omega=6.58$ μeV ($\omega=10$ GHz). Note the logarithmic scale; the inset shows the real part of the intraband conductivity on a linear scale, showing the linear dependence of σ on μ_c.

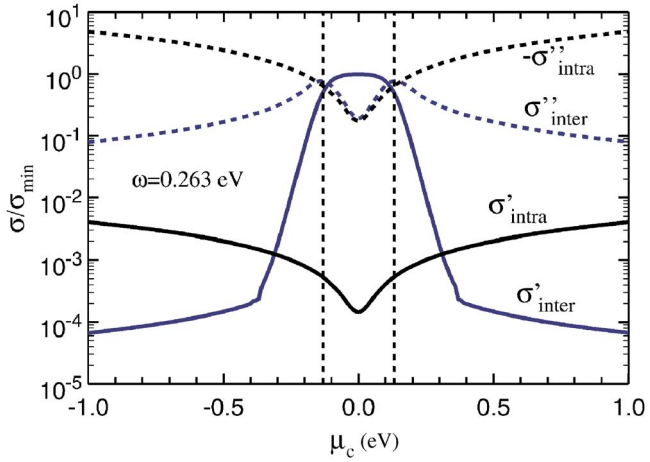

FIG. 5. (Color online) Intraband and interband conductivity as a function of chemical potential at $T=300$ K, $\omega=0.263$ eV ($\omega=400$ THz). The dashed vertical lines represent the point $2|\mu_c|=\hbar\omega$.

tenuation length are shown as a function of chemical potential at $\omega=6.58$ μeV. Because of the simple form for the TM surface-wave wavenumber (43), the wavenumber and attenuation length merely follow the conductivity profile.

However, at infrared frequencies moderate changes in the chemical potential can significantly alter graphene's conductivity and, significantly, change the sign of its imaginary part. Figure 5 shows the various components of the graphene conductivity at $\omega=0.263$ eV ($\omega=400$ THz), and in Fig. 6 the total conductivity (intraband plus interband) is shown. From Eq. (4), at $T=\Gamma=0$ an abrupt change in σ_{inter} occurs when $2|\mu_c|=\hbar\omega$, which in this case is $|\mu_c|=0.132$ eV, denoted by the vertical dashed lines in the figures. Since the associated Fermi temperature is several thousand K, the $T=0$ behavior qualitatively remains the same at 300 K, although the discontinuity is softened due to the higher temperature. It can be seen that for $|\mu_c|$ less than approximately 0.13 eV, σ''_{inter} dominates over σ''_{intra} and $\sigma''>0$, so that only a proper TE surface wave mode exists. Outside of this range, only a TM surface wave propagates. This is shown in Fig. 7, where it can be seen that the TM mode is moderately dispersive with chemical potential, especially in the region of the sign change in σ'' near $|\mu_c|\simeq 0.132$ eV, since the TM surface wave is fairly well confined to the graphene surface ($\zeta^{TM}/\lambda \leq 10^{-2}$). In the region where σ'' is positive, the TE mode exists but is poorly confined to the graphene surface, and so it is essentially nondispersive and very lightly damped. The oscillatory behavior of the attenuation length ζ^{TE} follows simply from the form of σ'' via Eq. (45).

In Fig. 8 the conductivity is shown as a function of frequency in the infrared regime for a fixed value of chemical potential, $\mu_c=0.1$ eV, at 300 K. The dispersion behavior of the conductivity follows simply from Eqs. (3) and (4). The point $2|\mu_c|=\hbar\omega$ occurs at $\omega=0.2$ eV ($\omega\simeq 301.6$ THz), whereupon the interband contribution dominates and σ'' becomes positive (the intraband contribution varies as ω^{-1} for $\omega\gg\Gamma$, and so becomes small at sufficiently high infrared frequencies). For comparison, the $T=0$ result is also shown.

Figure 9 shows the TM and TE wavenumbers and attenuation lengths for the conductivity profile given in Fig. 8.

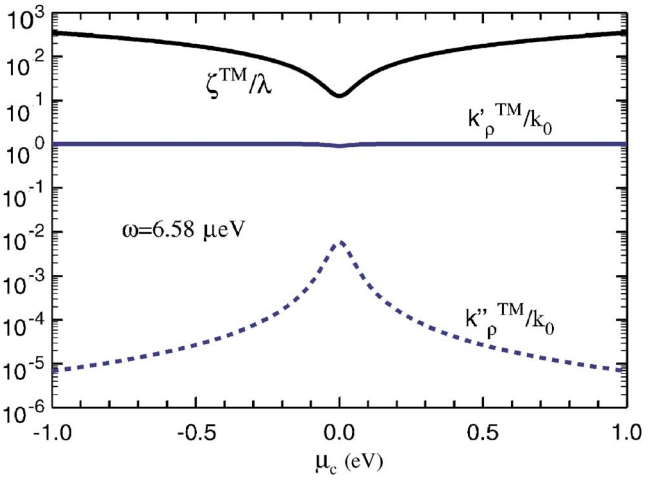

FIG. 4. (Color online) Attenuation length and surface-wave wavenumber for the TM mode as a function of chemical potential at $T=300$ K, $\omega=10$ GHz (6.58 μeV). The corresponding conductivity profile is shown in Fig. 3.

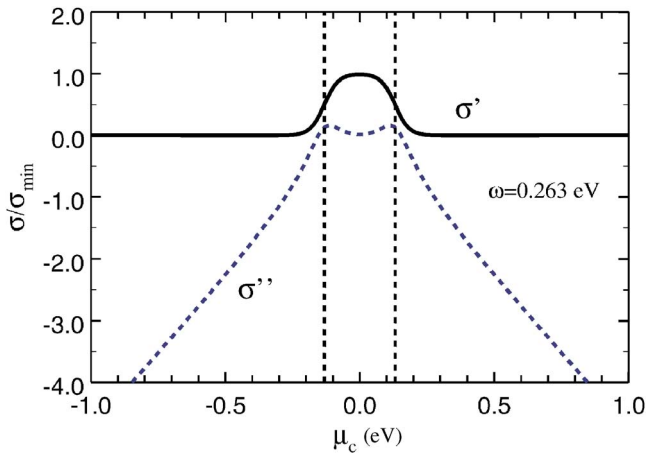

FIG. 6. (Color online) Total (intraband plus interband) conductivity as a function of chemical potential at $T=300$ K, $\omega=0.263$ eV ($\omega=400$ THz). The dashed vertical lines represent the point $2|\mu_c|=\hbar\omega$.

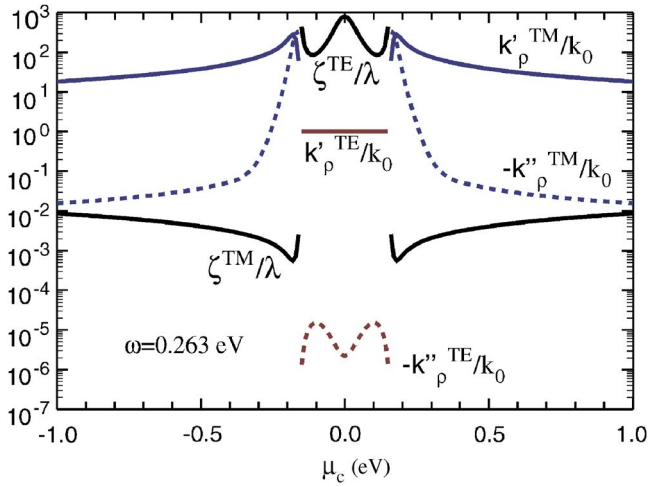

FIG. 7. (Color online) Attenuation length and surface-wave wavenumbers as a function of chemical potential at T=300 K, ω=0.263 eV (ω =400 THz). The corresponding conductivity profile is shown in Figs. 5 and 6. TE and TM modes are shown, although only portions where wavenumbers lie on the proper Riemann sheet are provided.

For $\omega<0.2$ eV only a TM surface wave exists since $\sigma''<0$, and for $\omega>0.2$ eV only a TE surface wave exists due to $\sigma''>0$. From Fig. 8 it is clear that above ω=0.1 eV, $|\sigma|\eta_0/2 \ll 1$, and so

$$k_\rho^{TM} = k_0\sqrt{1-\left(\frac{2}{\sigma\eta_0}\right)^2} \simeq -jk_0\left(\frac{2}{\sigma\eta_0}\right), \tag{47}$$

$$k_\rho^{TE} = k_0\sqrt{1-\left(\frac{\sigma\eta_0}{2}\right)^2} \simeq k_0\left[1-\frac{1}{2}\left(\frac{\sigma\eta_0}{2}\right)^2\right]. \tag{48}$$

The TM mode is tightly confined to the graphene surface, and from Eq. (47) it can be seen that in the vicinity of the transition point at ω=0.2 eV, where $\sigma''\simeq 0$, k_ρ'' will be large and the TM mode will be highly damped. Just to the right of the transition, from Eq. (48) the TE wavenumber is predominately real, and so the TE mode is very lightly damped. From Eq. (45) it is clear that $\zeta^{TE}/\lambda \gg 1$, and so the TE mode is not well confined to the surface in this frequency range.

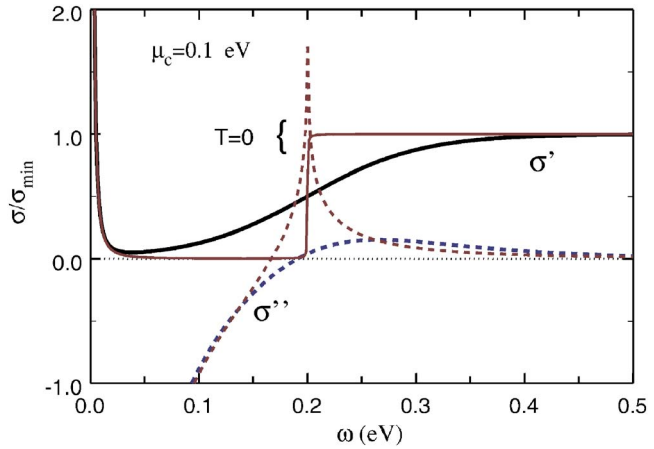

FIG. 8. (Color online) Total conductivity (intraband plus interband) as a function of frequency at T=300 K and μ_c=0.1 eV at infrared frequencies (ω=0.1 eV$\simeq$151.2 THz). The T=0 result is also shown for comparison.

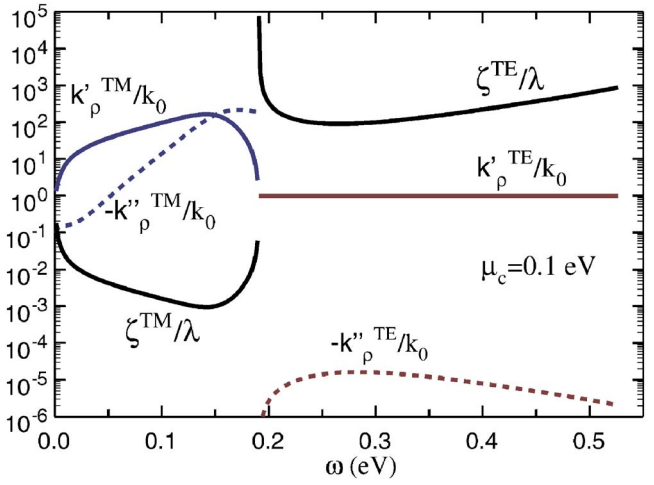

FIG. 9. (Color online) Attenuation length and surface-wave wavenumbers as a function of frequency at μ_c=0.1 eV, T=300 K. The corresponding conductivity profile is shown in Fig. 8.

IV. CONCLUSIONS

An exact solution has been obtained for the electromagnetic field due to an electric current near a surface conductivity model of graphene. Dyadic Green's functions have been presented in terms of Sommerfeld integrals, plane wave reflection and transmission coefficients have been provided, and surface wave propagation on graphene has been discussed in the microwave and infrared regimes. The relative importance of intraband and interband contributions for surface wave propagation has been emphasized.

[1]R. Saito, G. Dresselhaus, and M. S. Dresselhaus, *Physical Properties of Carbon Nanotubes* (Imperial College, London, 2003).
[2]C. Berger, Z. Song, T. Li, X. Li, A. Y. Ogbazghi, R. Feng, Z. Dai, A. N. Marchenkov, E. H. Conrad, P. N. First, and W. A. de Heer, J. Phys. Chem. **108**, 19912 (2004).
[3]Y. Zhang, J. P. Small, W. V. Pontius, and P. Kim, Appl. Phys. Lett. **86**, 073104 (2005).
[4]C. Berger, Z. Song, X. Li, X. Wu, N. Brown, C. Naud, D. Mayou, T. Li, J. Hass, A. N. Marchenkov, E. H. Conrad, P. N. First, and W. A. de Heer, Science **312**, 1191 (2006).
[5]K. S. Novoselov, A. K. Geim, S. V. Morozov, D. Jiang, Y. Zhang, S. V. Dubonos, I. V. Grigorieva, and A. A. Firsov, Science **306**, 666 (2004).
[6]K. S. Novoselov, A. K. Geim, S. V. Morozov, D. Jiang, M. I. Katsnelson, I. V. Grigorieva, S. V. Dubonos, and A. A. Firsov, Nature (London) **438**, 197 (2005).
[7]Y. Zhang, Y.-W. Tan, H. L. Stormer, and P. Kim, Nature (London) **438**, 201 (2005).
[8]J. Hass, R. Feng, T. Li, Z. Zong, W. A. de Heer, P. N. First, E. H. Conrad, C. A. Jeffrey, and C. Berger, Appl. Phys. Lett. **89**, 143106 (2006).
[9]Y. Ouyang, Y. Yoon, J. K. Fodor, and J. Guo, Appl. Phys. Lett. **89**, 203107 (2006).
[10]G. Y. Slepyan, S. A. Maksimenko, A. Lakhtakia, O. Yevtushenko, and A. V. Gusakov, Phys. Rev. B **60**, 17136 (1999).
[11]L. A. Falkovsky and S. S. Pershoguba, Phys. Rev. B **76**, 153410 (2007).
[12]S. A. Mikhailov and K. Ziegler, Phys. Rev. Lett. **99**, 016803 (2007).
[13]V. P. Gusynin and S. G. Sharapov, Phys. Rev. B **73**, 245411 (2006).
[14]V. P. Gusynin, S. G. Sharapov, and J. P. Carbotte, Phys. Rev. Lett. **96**, 256802 (2006).
[15]N. M. R. Peres, F. Guinea, and A. H. Castro Neto, Phys. Rev. B **73**, 125411 (2006).
[16]N. M. R. Peres, A. H. Castro Neto, and F. Guinea, Phys. Rev. B **73**, 195411 (2006).
[17]K. Ziegler, Phys. Rev. B **75**, 233407 (2007).
[18]L. A. Falkovsky and A. A. Varlamov, Eur. Phys. J. B **56**, 281 (2007).
[19]V. P. Gusynin, S. G. Sharapov, and J. P. Carbotte, J. Phys.: Condens.

Matter **19**, 026222 (2007).
[20]P. R. Wallace, Phys. Rev. **71**, 622 (1947).
[21]V. P. Gusynin, S. G. Sharapov, and J. P. Carbotte, Phys. Rev. B **75**, 165407 (2007).
[22]In previous theoretical studies of pure graphene at low temperatures there is some variation in the predicted value of conductivity (Ref. 17), although all methods predict conductivity on the order of e^2/h, in approximate agreement with Eq. (5). For example, the minimum conductivity measured in Ref. 6 (for temperatures less than approximately 100 K) was $\sigma = 4e^2/h$.
[23]W. C. Chew, *Waves and Fields in Inhomogeneous Media* (IEEE, New York, 1995).
[24]A. Ishimaru, *Electromagnetic Wave Propagation, Radiation, and Scattering* (Prentice Hall, Englewood Cliffs, NJ, 1991).
[25]J. S. Bagby and D. P. Nyquist, IEEE Trans. Microw. Theory Tech. **35**, 207 (1987).
[26]T. Tamir and A. A. Oliner, Proc. IEEE **110**, 310 (1963).
[27]R. A. Jishi, M. S. Dresselhaus, and G. Dresselhaus, Phys. Rev. B **48**, 11385 (1993).